Carbon 96 (2016) 311–315

Contents lists available at ScienceDirect

Carbon

journal homepage: www.elsevier.com/locate/carbon

Letter to the Editor

Fe-catalyzed etching of exfoliated graphite through carbon hydrogenation

A B S T R A C T

We present an investigation on Fe-catalyzed etching of graphite by dewetting Fe thin films on graphite in forming gas. Raman mapping of the etched graphite shows thickness variation in the etched channels and reveals that the edges are predominately terminated in zigzag configuration. X-ray diffraction and photoelectron spectroscopy measurements identify that the catalytic particles are Fe with the presence of iron carbide and iron oxides. The existence of iron carbide indicates that, in additional to carbon hydrogenation, carbon dissolution into Fe is involved during etching. Furthermore, the catalytic particles can be re-activated upon a second annealing in forming gas.

Since the early 1970s, it has been demonstrated that Fe is an active catalyst in etching channels in graphite [1,2]. With the emergence of exfoliated graphene, Fe-catalyzed carbon hydrogenation has been used to etch specific edges or nanoribbons in exfoliated graphene layers on a Si/SiO_2 substrate [3]. Meanwhile, advanced electron microscopy techniques such as electron tomography [4] and *in situ* Cs aberration-corrected transmission electron microscopy (TEM) [5] have been used to explore this catalytic etching process. In particular, electron tomography combined with high resolution TEM and spatial-resolved electron energy loss spectroscopy has been used to characterize the etched channels and catalytic particles and to obtain a real three-dimensional (3D) image of the cutting process [4]. *In situ* Cs aberration-corrected TEM has directly captured the catalytic removal and insertion of sp^2 carbon at graphene edges by a single Fe atom while under electron irradiation [5]. It has also revealed that the diffusion of single Fe atoms at the graphene edges is edge-dependent (zigzag and armchair), with subdiffusion being shown for armchair edge termination and superdiffusion being shown for zigzag termination [5]. This difference is attributed to different diffusion barriers between the edge terminations [5].

It is well known that, in the presence of hydrogen, the catalytic process is through carbon hydrogenation with the production of methane [1]. In our previous work [6], by dewetting Fe thin films on graphite, we produced catalytic particles not only at the step edges of graphite but also on the basal plane. The etched channels are observed in graphite flakes annealed in forming gas but not in those annealed in nitrogen [6]. Hydrogen plays a critical role in the etching of graphite under our reaction conditions, confirming that the etched channels in graphite are catalyzed by Fe particles through the hydrogenation of graphite. Meanwhile, as shown in the complex Fe–C phase diagram, carbon can dissolve into Fe at high temperatures and forms metastable iron carbide (Fe_3C, 6.67% carbon by weight) [6]. Iron carbide formation has been observed in the growth of carbon nanotubes through chemical vapor deposition using Fe as the catalyst [7]. Therefore, it is of great interest to determine whether iron carbide forms during the etching process.

In this work, we characterize etched graphite for the edge termination (whether the etched edges are predominately zigzag or armchair) and the catalytic particles for the carbide formation (whether carbon dissolution in Fe occurs) during carbon hydrogenation. Specifically, we characterize the etched graphite with Raman spectroscopy and the catalytic particles by X-ray diffraction (XRD) and X-ray photoelectron spectroscopy (XPS). Raman mapping provides information on the edge configuration for the etched edges and on the thickness variation in the etched channels. By comparing the Fe thin films on graphite annealed in forming gas with those annealed in nitrogen, XRD and XPS provide the chemical and crystalline information of the catalytic particles. Furthermore, we performed a second annealing in forming gas for the sample previously annealed in forming gas to track the particles which can be re-activated catalytically. With the new information, we gain a full understanding of catalytic carbon hydrogenation.

Graphite flakes were obtained by mechanically exfoliating from Kish graphite onto a Si substrate with a 300 nm SiO_2 layer. An Fe thin film (28 nm) was deposited onto these flakes by sputtering (Denton Vacuum Sputtering System, Discovery-550). Then the samples were loaded into a rapid thermal processor (Model 600xp, Modular Process Technology Corporation). The sample chamber was purged using nitrogen (10,000 sccm flow rate) for 1 min before the samples were rapidly heated to 950 °C in 90 s in

http://dx.doi.org/10.1016/j.carbon.2015.09.079
0008-6223/

forming gas (90% nitrogen and 10% hydrogen, 4000 sccm flow rate) and held at that temperature for 30 s. Afterwards, the system was rapidly cooled to room temperature in 180 s Fig. 1a shows an optical image of a large-area, exfoliated graphite region after the annealing of the Fe thin film at 950 °C for 30 s in forming gas. Etched tracks marked with the arrows in Fig. 1a appear on graphite. These etched tracks appear lighter than the neighboring graphite region in the In-lens low-voltage scanning electron microscopy (LVSEM, Zeiss, Ultra-60, 1 kV) image shown in Fig. 1b, indicating the removal of multiple graphene layers and the thinning of the graphite. Due to variation of the number of graphene layers removed, both images show color contrast along the same etched track (marked with the arrows in Fig. 1a) and among the different etched tracks.

We performed Raman spectroscopic measurements in the etched graphite region. Raman spectra were acquired under ambient conditions with a micro-Raman spectrometer (Renishaw InVia Raman system) equipped with a 514.5 nm (2.41 eV) wavelength excitation laser and an 1800 lines/mm grating while operating in 180° backscattering geometry. A 50× objective was used to focus the excitation laser to an approximately 1 μm spot onto the sample with an incident power of less than 2 mW to avoid local heating effects. Raman mapping was performed in the rectangle region (52 μm × 42 μm) shown in Fig. 1a with a step size of 1 μm and an exposure time of 1 s at each point. Fig. 1c shows the Raman map of the integrated G peak area (A(G), 1480 cm^{-1}–1680 cm^{-1}). The Raman map reveals variation of A(G) between the etched and non-etched graphite. It has been reported that, as the number of graphene layers increases from 1 to 100 layers, the intensity of G peak does not increase monotonically but the intensity of Si peak decreases monotonically [8]. Therefore, the variation in the number of graphene layers in the thin graphite flasks can be reflected by the variation in the intensity of Si peak from the Si substrate underneath the thin graphite flakes. The Raman map of the integrated Si peak area (A(Si), 420 cm^{-1}–620 cm^{-1}) from the Si substrate (Fig. 1d) shows the variation of A(Si) along the same etched channels (marked with the arrows in Fig. 1a) and among the different etched tracks due to the variation in the number of graphene layers removed.

Raman spectroscopy is also a powerful technique to identify the etched edges in graphene [9]. With the fulfillment of overall momentum conservation during the Raman scattering process, the Raman spectrum from an armchair edge has a prominent D peak, while, without the fulfillment of overall momentum conservation, no D peak is observed for a zigzag edge [9]. Fig. 1e shows the Raman map of the integrated D peak area (A(D), 1250 cm^{-1}–1450 cm^{-1}). Even though the overall A(D) is small, some of etched tracks are

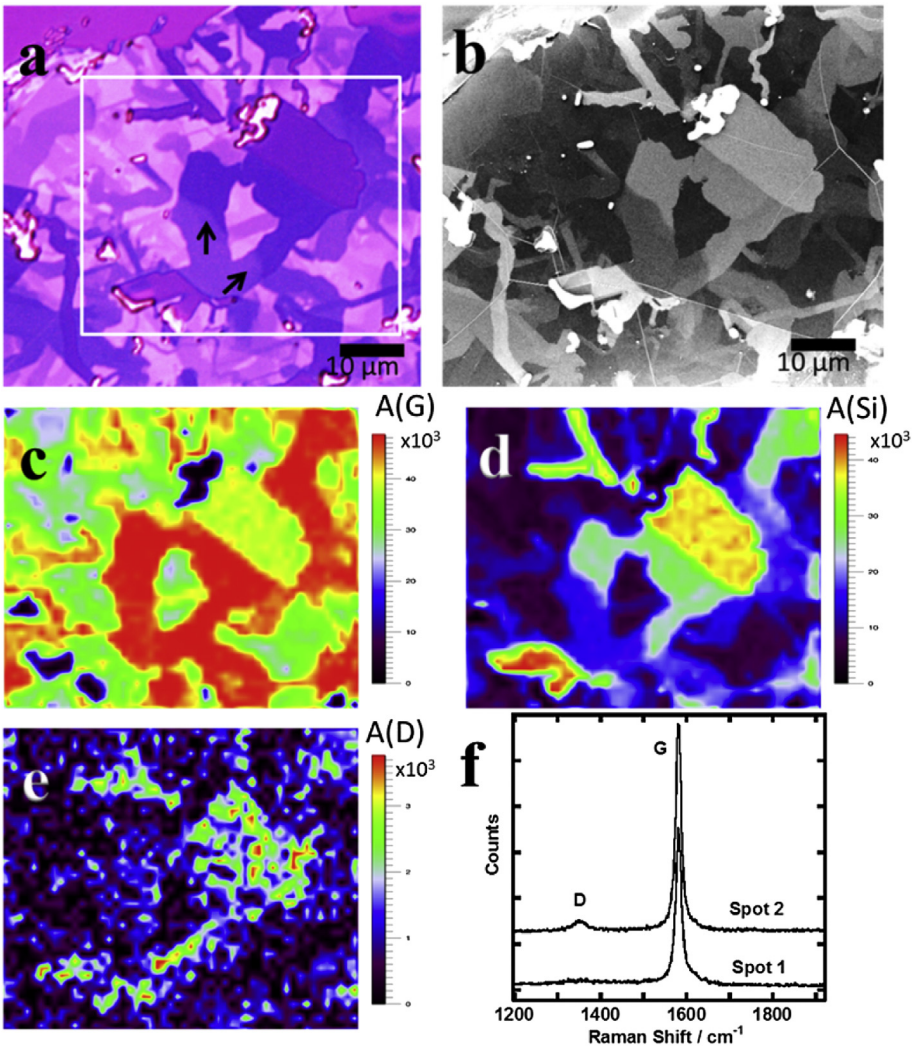

Fig. 1. Fe-catalyzed etching of graphite in forming gas. (a) Optical and (b) LVSEM images of graphite on a Si/SiO_2 substrate after annealing of the Fe thin film. (c–e) Raman maps for the rectangle region (52 μm × 42 μm) marked in (a) with integrated area of G, Si, and D peaks, respectively. (f) Micro-Raman spectra from two locations with slightly larger integrated area of D peak in (e). (A colour version of this figure can be viewed online.)

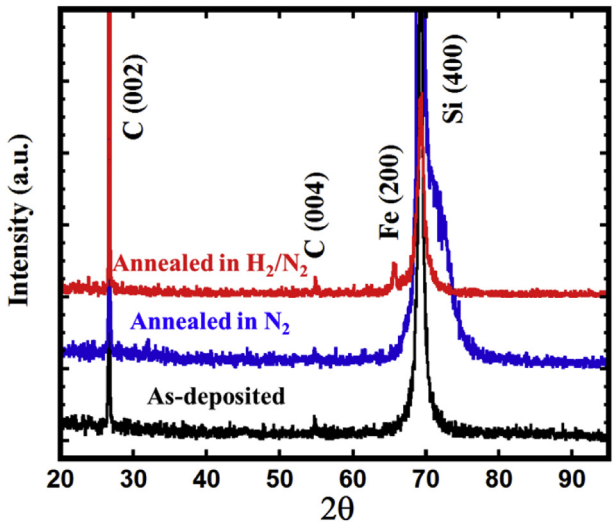

Fig. 2. X-ray diffraction patterns for the as-deposited Fe thin film and annealed samples in nitrogen or forming gas. (A colour version of this figure can be viewed online.)

highlighted with a slightly larger A(D). Fig. 1f shows two Raman spectra from two such locations. Even in these two locations, the D peak is relatively weak. Moreover, there is no large A(D) along the etched edges. Therefore, the etched edges for either straight or curvy tracks have predominately zigzag configuration, in accordance with the theoretical simulations showing that Fe atom has lower activation energy and diffusion barriers in unzipping graphene along a zigzag edge than along armchair edge [5].

In comparison, when the Fe thin film on graphite is annealed at 950 °C for 30 s in nitrogen (4000 sccm flow rate), we observed the formation of fractal-shaped particles through dewetting of the Fe thin film [6], indicating that the presence of hydrogen has an impact on the particle morphology. Also, no etching of graphite was observed. Even though we have shown that defects are introduced on the top layers of graphite by sputtering an Fe thin film [6], those defects alone clearly cannot initiate the etching of graphite in nitrogen under our reaction conditions. Hydrogen is critical for the formation of etched channels in graphite. Therefore, the etched channels in graphite in Fig. 1a are produced through the hydrogenation of graphite. Next, it is critical to investigate the chemical components and crystallinity of those catalytic particles to fully understand the catalytic process.

First, we carried out the XRD measurements (Rigaku X-ray diffractometer with Cu-Kα radiation) on the as-deposited Fe thin film and on those annealed in forming gas and in nitrogen. Fig. 2 displays their XRD patterns. Since the X-ray beam is large to cover the Fe thin film deposited on both graphite and the Si/SiO_2 substrate, three diffraction peaks centered at 26.7°, 54.8°, and 69.5° correspond to C(002), C(004), and Si(400), respectively. No diffraction peaks for Fe nor its oxides are observed in this XRD pattern.

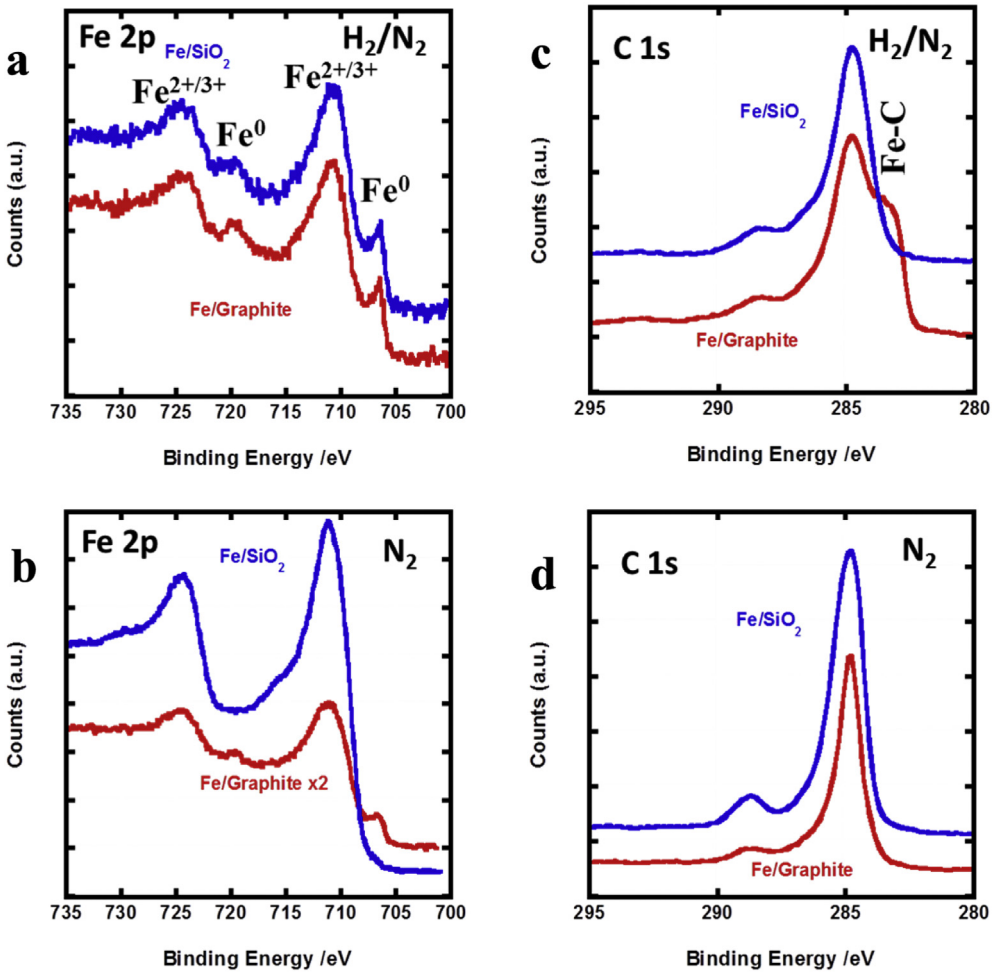

Fig. 3. High resolution X-ray photoelectron spectroscopy for the Fe thin film samples annealed in either forming gas or nitrogen. (a,b) Fe 2p region and (c,d) C 1s region. (A colour version of this figure can be viewed online.)

Therefore, the as-deposited Fe thin film is amorphous. For the Fe thin film annealed in nitrogen, the Si(400) peak is significantly broadened, indicating the induced change in Si substrate during the annealing process in nitrogen. For the Fe thin film annealed in forming gas, the Si (400) peak has similar shape and position to the as-deposited thin film. More importantly, a new diffraction peak centered at 65.0° appears and its position is close to that of body centered cubic α-Fe (200).

We further carried out XPS measurements (Kratos Axis instrument with mono-chromatized Al Kα excitation) on the particles on graphite and the Si/SiO_2 substrate produced in the two different gas environments. The analysis area of XPS is approximately 1 mm in diameter. Fig. 3a shows high resolution XPS data of the Fe 2p region for the sample annealed in forming gas. For particles on both graphite and the Si/SiO_2 substrate, the shape of their spectra is similar. The peaks at 706.6 eV (Fe^0 $2p_{3/2}$) and 719.5 eV (Fe^0 $2p_{1/2}$) indicate the existence of metallic Fe [10], further confirming that the peak at 65.0° observed in the XRD diffraction pattern is from metallic Fe. Meanwhile, the peaks at 710.8 eV (Fe^{2+}/Fe^{3+} $2p_{3/2}$) and 724.3 eV (Fe^{2+}/Fe^{3+} $2p_{1/2}$) indicate the formation of iron oxides [10]. For the sample annealed in nitrogen shown in Fig. 3b, the particles on graphite exhibit different spectral features from those on Si/SiO_2 substrate. While the particles on graphite show the existence of both metallic Fe and iron oxides, those on Si/SiO_2 substrate show the existence of only iron oxides. Considering the significantly broadened Si (400) peak shown in the XRD pattern for the Fe thin film annealed in nitrogen, the Fe thin films deposited on Si/SiO_2 regions likely react with SiO_2 and Si during the dewetting process. Even with the appearance of metallic Fe for the particles on graphite, no Fe diffraction peaks are observed, indicating those Fe particles are not crystalline. Therefore, the presence of hydrogen during the annealing process affects both the particles' morphology and crystallinity.

Fig. 3c and d show the high resolution XPS data of the C 1s region for the samples annealed in forming gas and in nitrogen, respectively. The four spectra exhibit similar features: 284.8 eV for adventitious carbon, 285–286 eV for C–O, and 288.5 eV for O–C=O [10]. Additionally, the particles on graphite annealed in forming gas exhibit a prominent shoulder peak at 283.3 eV, which corresponds to the carbon signal from iron carbide (Fe–C) [11] and indicates the formation of iron carbide in this region. Therefore, even though carbon is etched by forming methane through the reaction with hydrogen during the hydrogenation of graphite [1], iron carbide still forms through carbon dissolution into Fe.

During the annealing process in forming gas, catalytic particles are produced through dewetting of the Fe thin film. We further performed a second annealing on the sample with etched graphite at 950 °C for 30 s in forming gas to track the catalytic activity of the particles that were formed during the first annealing process. We compared the optical images of the same graphite regions to identify the changes in etching of graphite (Fig. 4). In the graphite region shown in Fig. 4a and b, most particles appear inactive within a short annealing time of 30 s, while three particles (~350 nm) marked with circles in Fig. 4a continue etching graphite but in different directions. In another region shown in Fig. 4c and d, larger particles (~10 μm) marked with the two circles in Fig. 4c continue etching graphite along the same directions. Therefore, both small and large particles produced during the first annealing process can be reactivated during a second annealing process. Meanwhile, by comparing Fig. 4c with Fig. 4d, we notice the surface changes associated with twin bands, which are readily produced during the process of cleaving graphite and correspond to mis-oriented regions in the basal plane between two tilt boundaries [12]. They appear as straight lines on the basal plane (marked with the arrows in Fig. 4c) and are typically along the crystallographic directions. After a second annealing, the twin bands marked in Fig. 4c disappear and new twin bands appear (marked with the arrows in Fig. 4d).

In summary, we present an investigation of Fe-catalyzed etching of exfoliated graphite through carbon hydrogenation. We characterize etched graphite by Raman mapping to show thickness

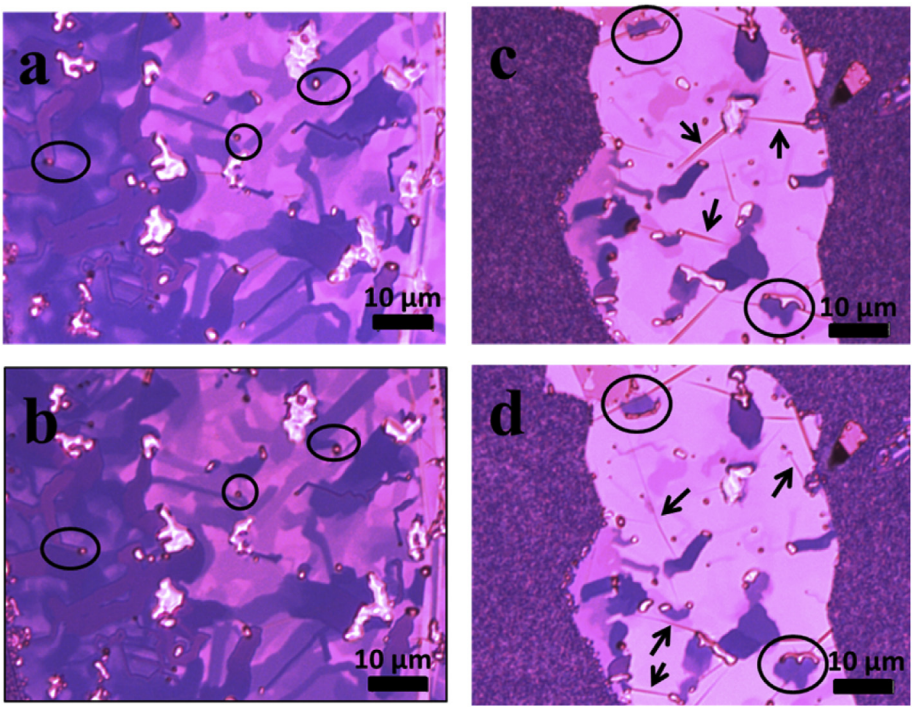

Fig. 4. Optical images of two graphite flakes. (a, c) after the first annealing of the Fe thin film in forming gas. (b, d) after a second annealing. (A colour version of this figure can be viewed online.)

variation in the etched channels and to determine that the etched edges are predominately terminated in zigzag configuration. Compared with the catalytic particles produced from annealing the Fe thin film in forming gas, the particles produced from annealing the Fe thin film in nitrogen are inactive in etching graphite under our reaction conditions. XRD and XPS measurements provide the chemical and crystalline information for the catalytic particles and identify them to be Fe particles with the presence of iron carbide and iron oxides. Even though the etching process involves the hydrogenation of graphite, iron carbide still forms through carbon dissolution into Fe. The presence of hydrogen during the annealing of the Fe thin film affects the resulting particles' morphology and crystallinity. Therefore, hydrogen is critical not only for the hydrogenation of graphite but also for the production of catalytic particles through the dewetting of the Fe thin film. We also demonstrate that, upon a second annealing in forming gas, particles can be re-activated catalytically and twin bands can be annihilated and created. These results provide new insights into the catalytic etching of graphite by Fe particles.

Acknowledgment

I. C. was partially supported by the National Research Council. Research performed in part at the NIST Center for Nanoscale Science and Technology. The authors thank Dr. Taner Yildirim for his help with XRD measurements. We identify certain commercial equipment, instruments, or materials in this article to specify adequately the experimental procedure. In no case does such identification imply recommendation or endorsement by the National Institute of Standards and Technology, nor does it imply that the materials or equipment identified are necessarily the best available for the purpose.

References

[1] A. Tomita, Y. Tamai, Optical microscopic study on catalytic-hydrogenation of graphite, J. Phys. Chem. 78 (22) (1974) 2254–2258.
[2] R.T.K. Baker, J.J. Chludzinski, R.D. Sherwood, A comparison of the catalytic influence of nickel, iron and nickel iron on the gasification of graphite in various gaseous environments, Carbon 23 (3) (1985) 245–254.
[3] S.S. Datta, D.R. Strachan, S.M. Khamis, A.T.C. Johnson, Crystallographic etching of few-layer graphene, Nano Lett. 8 (7) (2008) 1912–1915.
[4] G. Melinte, I. Florea, S. Moldovan, I. Janowska, W. Baaziz, R. Arenal, et al., A 3D insight on the catalytic nanostructuration of few-layer graphene, Nat. Commun. 5 (2014) 4109.
[5] J. Zhao, Q.M. Deng, S.M. Avdoshenko, L. Fu, J. Eckert, M.H. Ruemmeli, Direct in situ observations of single Fe atom catalytic processes and anomalous diffusion at graphene edges, Proc. Natl. Acad. Sci. U. S. A. 111 (44) (2014) 15641–15646.
[6] G.J. Cheng, I. Calizo, A.R.H. Walker, Metal-catalyzed etching of graphene governed by metal-carbon interactions: a comparison of Fe and Cu, Carbon 81 (2015) 678–687.
[7] V. Jourdain, C. Bichara, Current understanding of the growth of carbon nanotubes in catalytic chemical vapour deposition, Carbon 58 (2013) 2–39.
[8] X.-L. Li, X.-F. Qiao, W.-P. Han, Y. Lu, Q.-H. Tan, X.-L. Liu, et al., Layer number identification of intrinsic and defective multilayered graphenes up to 100 layers by the raman mode intensity from substrates, Nanoscale 7 (17) (2015) 8135–8141.
[9] B. Krauss, P. Nemes-Incze, V. Skakalova, L.P. Biro, K. von Klitzing, J.H. Smet, Raman scattering at pure graphene zigzag edges, Nano Lett. 10 (11) (2010) 4544–4548.
[10] G. Bhargava, I. Gouzman, C.M. Chun, T.A. Ramanarayanan, S.L. Bernasek, Characterization of the "native" surface thin film on pure polycrystalline iron: A high resolution XPS and TEM study, Appl. Surf. Sci. 253 (9) (2007) 4322–4329.
[11] D.Q. Yang, E. Sacher, Characterization and oxidation of Fe nanoparticles deposited onto highly oriented pyrolytic graphite, using X-ray photoelectron spectroscopy, J. Phys. Chem. C 113 (16) (2009) 6418–6425.
[12] E.J. Freise, A. Kelly, Twinning in graphite, Proc. Roy. Soc. A 264 (1317) (1961) 269–276.

Guangjun Cheng*, Irene Calizo[1], Christina A. Hacker, Curt A. Richter, Angela R. Hight Walker
Semiconductor and Dimensional Metrology Division, Physical Measurement Laboratory, National Institute of Standards and Technology, Gaithersburg, MD 20899, USA

* Corresponding author.
E-mail address: guangjun.cheng@nist.gov (G. Cheng).

16 June 2015
Available online 25 September 2015

[1] Current address: Department of Electrical and Computer Engineering, Florida International University, Miami, FL 33174, USA.